Residence time distributions for in-line chaotic mixers

Nelson Poumaëre ⬤, Benoît Pier ⬤, and Florence Raynal ⬤*

Laboratoire de Mécanique des Fluides et d'Acoustique, Université de Lyon,
École centrale de Lyon, INSA Lyon, Université Claude Bernard Lyon 1, CNRS, F-69134 Écully, France

We investigate the distributions of residence time for in-line chaotic mixers; in particular, we consider the Kenics, the F-mixer, and the multilevel laminating mixer and also a synthetic model that mimics their behavior and allows exact mathematical calculations. We show that whatever the number of elements of mixer involved, the distribution possesses a t^{-3} tail, so that its shape is always far from Gaussian. This t^{-3} tail also invalidates the use of second-order moment and variance. As a measure for the width of the distribution, we consider the mean absolute deviation and show that, unlike the standard deviation, it converges in the limit of large sample size. Finally, we analyze the performances of the different in-line mixers from the residence-time point of view when varying the number of elements and the shape of the cross section.

I. INTRODUCTION

Efficient stirring is the key ingredient of good mixing. This mechanism is generally associated with a turbulent flow, but even when the flow field is laminar, dynamical systems theory allows chaotic trajectories by stretching and folding of fluid elements, a process called chaotic advection [1–3]. Chaotic advection arises in a large diversity of natural or industrial flows. Extreme examples are mixing in geophysical flows (in the oceans [4] or magma in the earth mantle [5]), where the typical length scale reaches hundreds of kilometers, and microfluidics [6,7], with typical length scale of the order of $100\,\mu$m, that is, nine orders of magnitude smaller.

In this article, we are interested in in-line mixers, consisting of a succession of identical elements, which have applications from millifluidics [8,9] to microfluidics [10]. Although solving the concentration field is not easy to achieve because of their complicated geometry [11,12], it is well known that those mixers achieve a very good mixing by reproducing the baker's map. Thus they can indeed be considered as ideal mixers.

The present investigation focuses on another aspect of in-line mixers, their residence-time distributions (RTD) [13,14]: An ideal mixer is characterized by a very narrow Gaussian or a Dirac centered on the mean travel time. However, when considering only one element of an in-line mixer, the histogram of residence time is very broad and often monotonously decaying, with a maximum equal (or very close) to the minimum time involved to cross the element [15]: a behavior very far from that of an ideal mixer. Our goal is thus to study how the histogram evolves when increasing the number of elements.

Residence time distribution is a complex feature, not always correctly comprehended. Indeed, let us consider the case of the flow in a cylindrical pipe with circular cross section. The parallel flow field in the x direction is a parabolic profile

of equation:

$$v_x(r) = 2\,v_m\,(1 - r^2/R^2), \tag{1}$$

where r is the radial distance to the center of the section, R is the radius of the pipe, and v_m the mean velocity over the section. Because of the cylindrical symmetry, the residence time t depends only on r as

$$t(r) = L/v_x(r), \tag{2}$$

for a section of length L. Suppose now that we calculate the mean residence time t_m just by sampling randomly M particles at the inlet section at $t = 0$ (what Danckwerts named a "pulse signal" [14]) and measure the mean of the M corresponding residence times t. The result should be the same as what is obtained from the continuous equation:

$$t_m = \frac{1}{\pi R^2} \int_0^R t(r)\,2\pi r dr, \tag{3}$$

$$= \frac{L}{2v_m} \int_0^R \frac{1}{1 - r^2/R^2}\,\frac{2rdr}{R^2}, \tag{4}$$

$$= \frac{L}{2v_m} \int_0^1 \frac{1}{1 - u}\,du, \tag{5}$$

where we have used Eq. (2) and set $u = r/R$. Finally t_m diverges logarithmically when u approaches 1 (r approaches R), so that the mean time calculated this way is not defined. The reason lies in the way the mean time is calculated: When considering the inlet section during a lapse of time dt, many more particles cross at the center (where the velocity is maximal) than near the walls (where the velocity is very weak). As expressed by Danckwerts [13], "there is a variation in velocity from the axis to the wall of the pipe, so that the central 'core' of fluid moves with a velocity greater than the mean, while the fluid near the wall lags behind." In order to calculate a mean time, this nonuniform flux of particles must be taken into account by properly weighting the statistics [15–17]. As the quantity of particles that cross a section during dt is proportional to the crossing velocity, the weight must also be chosen proportional to this velocity, i.e., $v_\perp/v_m$ where

---

*Corresponding author: florence.raynal@ec-lyon.fr

$v_\perp$ is the component of the velocity perpendicular to the cross section. Now calculating again the mean time t_m using this weight, with $v_\perp = v_x$, leads to the trivial expression

$$t_m = \frac{1}{\pi R^2} \int_0^R \frac{v_x(r)}{v_m} t \, 2\pi r \, dr = L/v_m \qquad (6)$$

because of Eq. (2). We finally obtain the desired result,

$$t_m = \frac{\mathcal{V}}{Q}, \qquad (7)$$

where $\mathcal{V}$ is the volume of an element and Q the flow rate.

In a former article [15], we proposed to use the time of flight in order to obtain statistics of residence time. The time of flight is the lapse of time between the inlet and outlet of a given element when following a single fluid particle. Unlike RTD, the time of flight is a Lagrangian quantity, very close to the time of first return [18], or to the waiting time (time spent by a particle in a given domain $\mathcal{D}$) [19], both introduced for dynamical systems. Obviously, a particle trajectory is more likely to enter a given element in regions of high velocity than near the walls, so that there is no need for weighting the statistics as for RTD: When averaged, the time of flight converges naturally toward the mean time $t_m = \mathcal{V}/Q$ [15].

In the following, we will use time of flight to construct residence time distributions. The flow field is laminar, and we mostly consider nondiffusive particles, which corresponds to flows at high Péclet numbers on short times, for which the effects of molecular diffusion are negligible. The mean residence time in n elements is denoted by $t_m^{(n)} = n \times t_m$, where $t_m \equiv t_m^{(1)}$ is the mean residence time in a single element of mixer; similarly, $t_{\min}^{(n)} = n \times t_{\min}$ denotes the minimal time taken by a particle to cross n elements; the maximum time is infinite, due to the zero-velocity field on the walls. The density probability of residence time in n elements is denoted by $f_n(t)$.

This paper is organized as follows: In the next section we present the different mixers studied. We begin with the real mixers and show that their autocorrelation coefficient decreases very rapidly with the number of elements. This allows us to introduce a kinematic model that mimics the residence time distributions in a single element. In the following section we vary the number of mixing elements from 1 to n. In particular, we show that t^{-3} tail that exists for 1 element persists when the number of elements is increased. Then we explain how, because of this t^{-3} tail, the use of the classic standard deviation is forbidden. We thus discuss how to measure the stretching of RTD and choose the mean absolute deviation; we can therefore compare the different in-line mixers. Finally, in the last section we use this tool to discuss the influence of the cross-section geometry of mixing elements in the stretching of RTD.

II. MIXERS STUDIED

The mixers studied here—the Kenics, the F-mixer, and the multilevel laminating mixer (MLLM)—enable global chaos [15]; they are constituted of n identical elements. For each mixer we calculate the RTD using time of flight: We follow a fluid particle over time and record the time taken to cross each element. For the calculation of the time of flight in n elements, we sum the n individual times of flight corresponding to n elements in a row.

A. Real mixers

The numerical treatment of the velocity field by finite-element method and integration of the trajectories by a fourth-order Runge-Kutta method for the mixers studied here was explained in detail in Ref. [15]; we use the same numerical data here.

The computational geometries for three mixers are depicted in Fig. 1. The corresponding Poincaré sections and Lyapunov exponents are not shown here but can be found in Ref. [15]. A particle which exits at the outlet cross section of a computational geometry is reintroduced at the same location in the inlet cross section. This enables us to follow a particle on a very long number of elements, and we note the consecutive residence time in each element. Note that the number of elements involved in the computational geometries is not significant in this study.

For each mixer four long trajectories were calculated. A trajectory is terminated when the point ends in a wall, which may happen due to intrinsically limited numerical accuracy, or when a point is so close to a wall that the time taken to escape the element is too high. For this work the loss of particles is less than 1% [15].

The Kenics mixer [20] is composed of a series of identical internal blades inside a circular pipe; each blade has a helical shape, alternately right or left handed, and the leading edge of a given blade is at right angle of the trailing edge of the preceding blade. The computational geometry used here is shown in Fig. 1(a): Note that six elements are represented, so that the periodicity of the flow arises after two elements.

The MLLM [21–23] has a three-dimensional configuration intended to mimic the baker's map. The computational geometry used is shown in Fig. 1(b), with six elements represented. The successive elements are inverted so as to break the symmetry of the flow and avoid small residual nonchaotic regions [22]. Therefore here again, the structure has a periodicity of two elements.

Finally, the F-mixer [24,25] has a similar topological behavior as the MLLM, although its geometry is simpler; compared to the former, it is less symmetric, which is not a problem for Stokes flows. Indeed, its Lyapunov exponent is, as for the MLLM, equal to $\ln 2$ [15]. Its computational geometry is represented in Fig. 1(c), with eight elements. However, compared to the former, a mixing element represents a whole spatial period of the mixer. This property will be taken into account later.

B. Autocorrelation coefficient

How is a time of flight of a given element correlated to the time of flight in an element further away? It can be estimated through the autocorrelation coefficient,

$$R(i) = \frac{M}{M - i} \frac{\sum_{j=1}^{M-i}(t_j - t_m)(t_{j+i} - t_m)}{\sum_{j=1}^{M}(t_j - t_m)^2}; \qquad (8)$$

here $i = 1$ corresponds to the correlation between two consecutive elements. In Fig. 2 we have plotted the autocorrelation coefficient for the three mixers depicted above. As can be seen the time of flight decorrelates very rapidly with the number of elements.
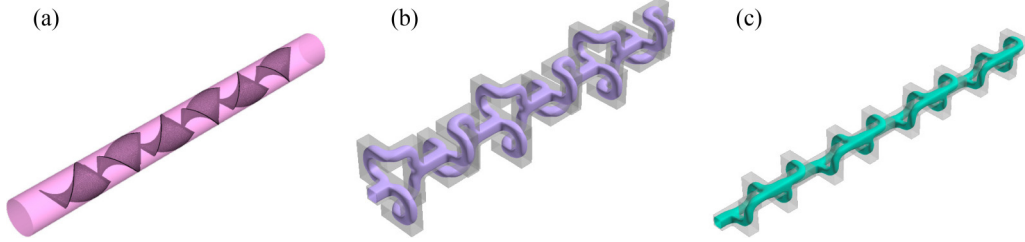
FIG. 1. Computational geometry of the different mixers studied: (a) the Kenics mixer (six elements); (b) the MLLM (six elements); (c) the F-mixer (eight elements). For (b) and (c) an isosurface of velocity modulus for a Stokes flow is plotted in color.

The decorrelation is the fastest for the F-mixer. Indeed, unlike the MLLM, its asymmetry leads to very different times of flight depending on the branch chosen in an element. Furthermore, as already noted, one element of the F-mixer corresponds to a full spatial period, in contrast to the two other mixers. But, even when considering this particularity, the decorrelation is still the fastest, since $R(1)$ is nearly zero, thus below $R(2)$ for the two other mixers.

Overall, for all mixers, the time of flight is totally decorrelated after only four basic elements. This rapid decorrelation of time of flight justifies *a priori* the model that we present hereafter.

C. A residence time model

We propose to model residence time in such mixers using the time of flight between inlet and outlet of an element with simple geometry. Such a model was previously used to model the distribution of time of flight in a single element of mixer [15]. It can be described as follows:

(i) the flow through one element of the mixer is modeled by a nonchaotic flow possessing no-slip boundaries (for instance a piece of pipe with circular cross section);

(ii) the effect of global chaos on the trajectory of the fluid particle is modeled by random reinjection at the entry to the next element with a probability density taking into account the fact that the particle randomly samples the whole section but less near the walls;
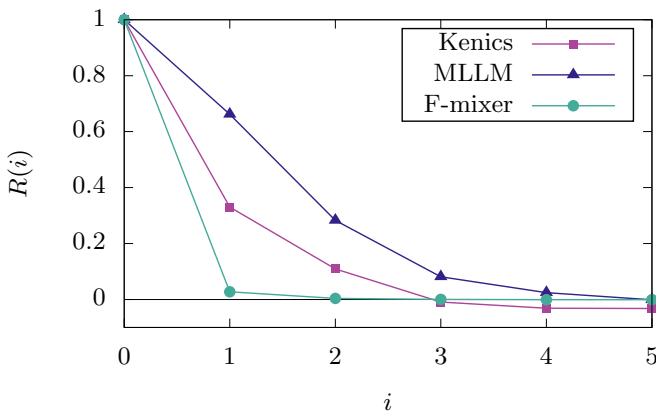

FIG. 2. Evolution of the correlation coefficient $R(i)$ between residence time values in elements that are i elements away for the three real mixers.

(iii) in order to conserve mass, as explained in the Introduction, the probability density function of the location of reinjection is taken proportional to the local velocity [see Eq. (9) below for a pipe with circular cross section].

In the following, we mostly focus on the case of a circular cross section (other shapes are also considered, see Sec. V). In practice we generate random numbers with a parabolic probability density using an inversion method [26], see Appendix A.

The circular cross section enables indeed an analytical expression for the probability density $f_1(t)$ to have a time of flight of duration t for 1 element: The probability to have a duration of time in between t and $t + dt$ is equal to that of having a particle reinjected in between r and $r + dr$, where t and r are linked by relation (2):

$$f_1(t)\, dt = \frac{v_x(r)}{v_m} \frac{2\pi r\, dr}{\pi R^2}, \tag{9}$$

where $v_x(r)$ verifies Eq. (1). When differentiating Eq. (2), we obtain

$$-\frac{2r\, dr}{R^2} = -\frac{L}{2 v_m t^2} dt, \tag{10}$$

which, when combined with Eqs. (9), (2), and (6), leads to

$$f_1(t) = \frac{t_m^2}{2t^3}. \tag{11}$$

This is indeed the profile obtained numerically for one element, see Fig. 3(a). Not surprisingly, the expression derived by Danckwerts [13] is recovered. This t^{-3} tail was also found for the three mixers in the case of a single element ($n = 1$). Because large times of flight correspond to points located near the wall where the velocity is weak, this behavior was related to the region of constant shear near the wall [15]. An indirect proof can be found when considering the plane Couette flow, where the shear is constant everywhere: For this flow also, the probability density follows Eq. (11) [15].

In the following, we propose to use this model for n consecutive elements of an in-line mixer.

III. RESIDENCE TIME DISTRIBUTIONS: FROM 1 TO n MIXING ELEMENTS

For a single-element of mixer, the RTD is characterized by the following properties [15]:

the existence of a t^{-3} tail and a maximum close to $t = t_{\min}$.

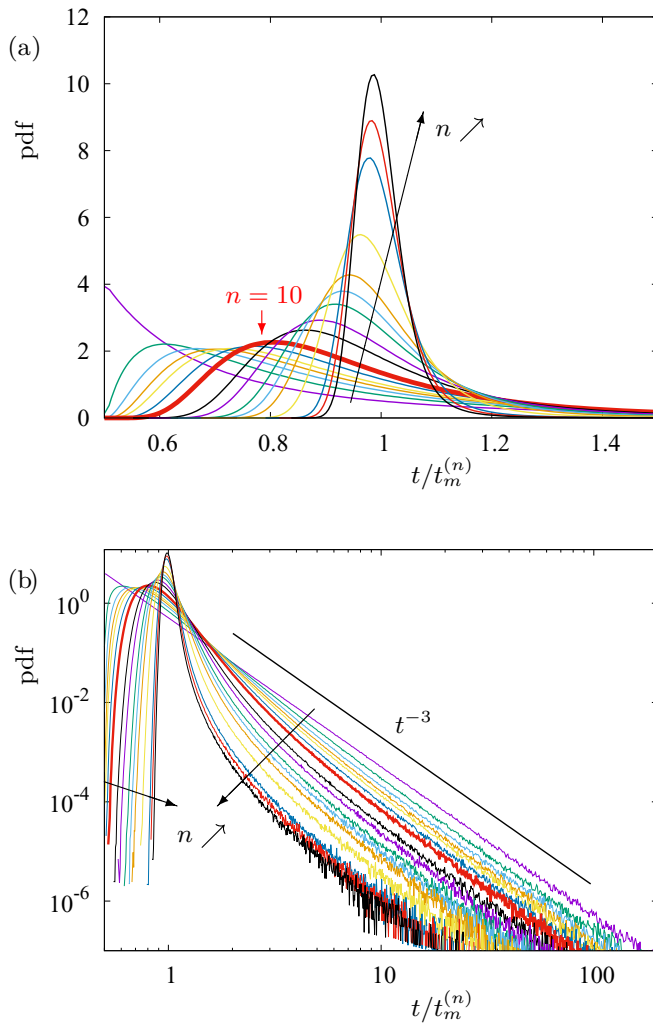As already stated, our idea is now to go further and explore the more realistic case of multiple elements.

FIG. 3. Residence time distribution f_n for the model chaotic flow (Poiseuille flow with circular cross section) for different numbers of sections, $n = 1, 2, 3, 4, 5, 7, 10, 14, 20, 30, 50, 70, 100, 140, 200, 300, 500, 700$, and 1000. By way of comparison with real mixers, the case $n = 10$ is drawn thicker. Each distribution was built with $M = 10^8$ data; the data are the sum of n independent residence times. (a) Linear scale; (b) logarithmic scale. Even for a very large number of sections n, the probability density function (pdf) is far from Gaussian, and exhibits a t^{-3} power-law tail. For the large number of elements, the tails are slightly more scattered, because more points are in the peak [Fig. 3(a)].

A. Model

The model is of particular interest since, because of its intrinsic simplicity, it allows to increase arbitrarily the number of elements. In Fig. 3(a) we show the nondimensional time distributions [built as a nondimensional probability density function (pdf)] for a number of elements varying from $n = 1$ to $n = 1000$. Of course, 1000 elements is not a realistic configuration in practice, but it allows us to visualize theoretically the rate of convergence toward the "perfect" mixer.

The first notable point is that for $n \geqslant 2$ the distribution is actually a bell curve, with a maximum different from $t = t_{\min}$, therefore a much improved shape compared to the $n = 1$ case. When n increases the curve becomes more peaked, and the

position of the maximum tends to the mean time of flight $t_m^{(n)} = n \times t_n^{(1)}$. However, the convergence is very slow. The case $n = 10$, that can be considered as a reasonable maximum number of elements in a real mixer, is shown as a thicker line (in red): As can be seen, the distribution is still very broad; furthermore, even for $n = 1000$, the maximum of the distribution is still not completely centered on the mean time.

The second notable point is visible in the log-log plot of the same distributions [Fig. 3(b)]: The t^{-3} tail that was found for $n = 1$ persists at all higher values of n, and the distributions remain very asymmetric. In the model, all residence times in an element are completely independent of each other. It can be shown that the distribution of the sum of two decorrelated data with an algebraic tail also possesses an algebraic tail [27,28]. In Appendix B, we apply this result and prove the existence of this t^{-3} tail when summing n independent data taken from the same distribution with a t^{-3} tail.

In real mixers, two consecutive times are not completely decorrelated as in the model (Fig. 2). However, because the correlation is weak, quite similar results are expected.

B. Mixers

Figure 4 shows the RTD for the three mixers. Due to a much reduced number of data points for the real mixers compared to the model, the histograms are limited to distributions for $n = 10$ elements; in any case, most in-line mixers have fewer than 10 mixing elements.

As expected, the distributions are quite similar to what was obtained with the model, although not as smooth, due to the much smaller sample of data. As for the model, the distributions are still broad for $n = 10$ and quite far from the desired Gaussian shape. Another important point is the persistence of the t^{-3} tail, visible on the log-log plot. This is not surprising: We demonstrated that summing n independent variables with a t^{-3} tail led to a distribution with a similar tail. These real-mixer data are poorly correlated (see Fig. 2), so that the variables may be considered as nearly independent. The assumption of uncorrelated data is almost exact for the F-mixer, for which the autocorrelation coefficient has fallen to negligible values after only one element. Moreover, the least noisy tail is that of the MLLM [Fig. 4(d)], for which we have twice as much data as for the two other mixers but that also corresponds to the more correlated mixer. Finally, note that El Omary *et al.* [29] also found a t^{-3} tail when properly weighting their statistics.

A distribution with an algebraic tail $t^{-\alpha}$ (also called Pareto distribution) belongs to the family of "heavy-tailed" distributions [30]. This type of distribution is well known in economy [31], finance [32], physics [33], maths [34], and even bibliometry [35].

IV. A MEASUREMENT TOOL FOR THE STRETCHING OF RESIDENCE TIME DISTRIBUTION

A. Why not use the standard deviation?

When dealing with distributions it is natural to measure the histogram width. Because many distributions in fluid mechanics are Gaussian, or close to Gaussian, it is usual to use
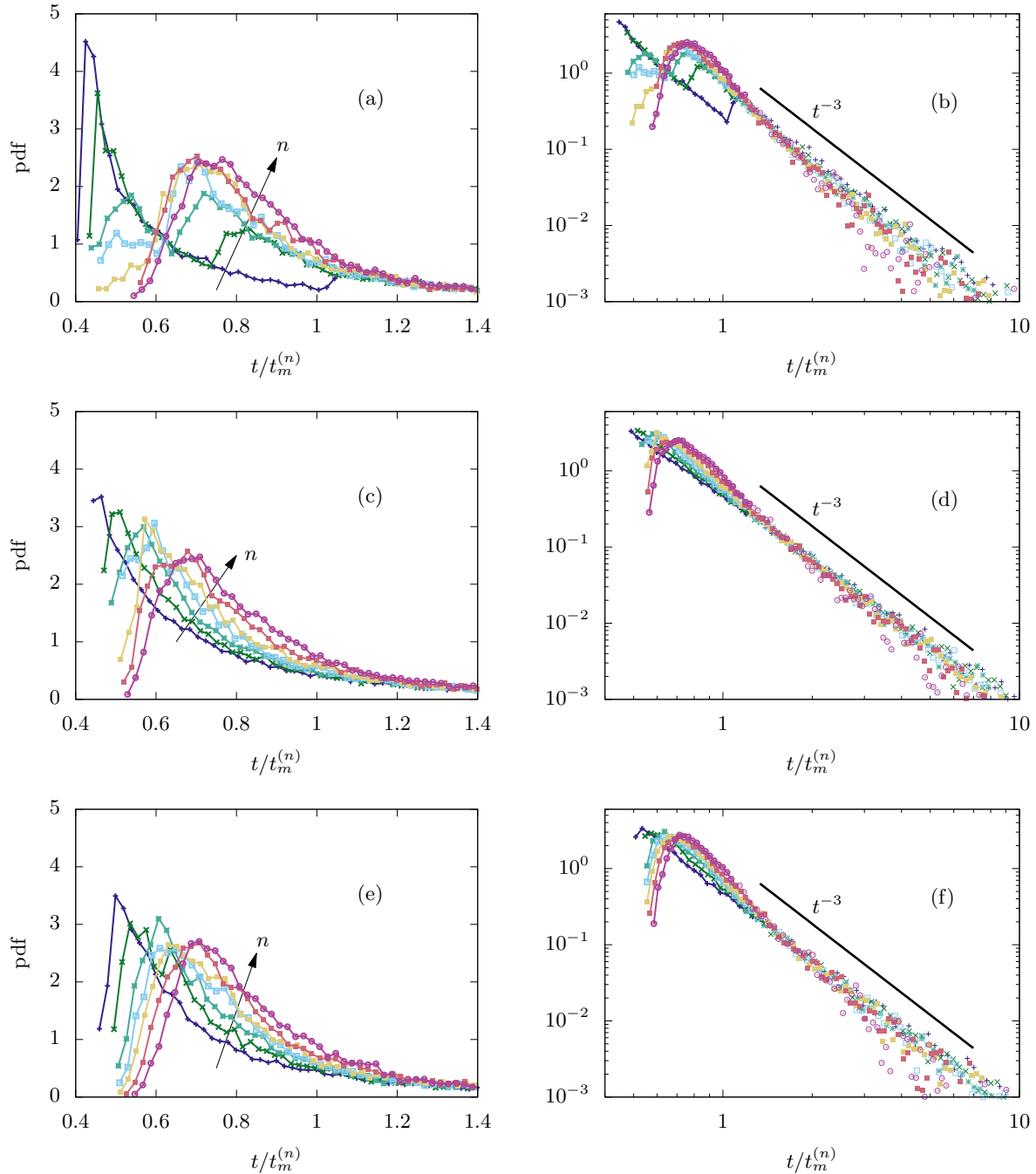
FIG. 4. Residence time distributions for the three real mixers for different numbers of elements, $n = 1, 2, 3, 4, 5, 7, 10$. From top to bottom: Kenics, MLLM, and F-mixer. For each mixer, four trajectories were calculated, corresponding to a total of 16 886 times of flight for the Kenics, 33 570 for the MLLM, and 18 987 for the F-mixer. We used a sliding average, so that the number of points are roughly the same for the different values of n. Left: linear scale; right: logarithmic scale. As for the model, the tail is more noisy for the highest values of n ($n \geqslant 7$): The weight (integral under the curve) of the bell-shaped part is more significant, which implies that the proportion of points in the tail is less important.

the standard deviation, or even higher moments. In our case, the standard deviation for n consecutive elements is denoted by $\sigma_2^{(n)}$ and defined as:

$$\sigma_2^{(n)} = \sqrt{\int_{t_{\min}^{(n)}}^{\infty} f_n(t) \left[\frac{t}{t_m^{(n)}} - 1 \right]^2 dt} \,. \qquad (12)$$

However, because of the t^{-3} tail, the integral diverges and this quantity is clearly not well defined.

It is always possible in practice to calculate a standard deviation from a series of M values of time of flight as:

$$\sigma_2^{(n)} = \sqrt{\frac{1}{M} \sum_{j=1}^{M} \left[\frac{t_j}{t_m^{(n)}} - 1 \right]^2} \,. \qquad (13)$$
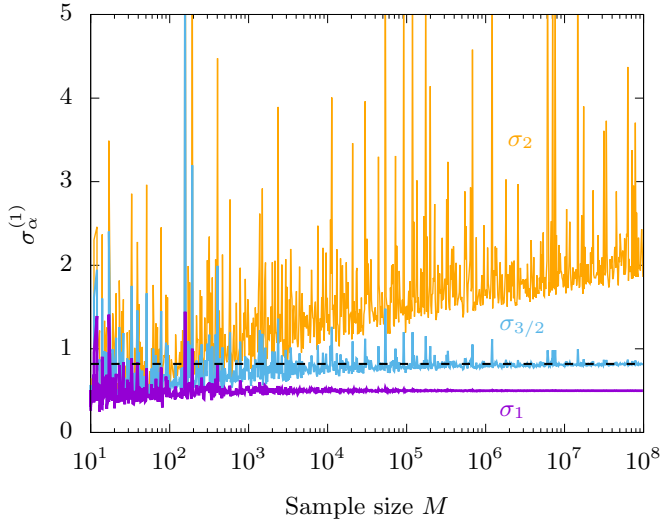
FIG. 5. Evolution of the standard deviation σ_2 (orange), centered absolute moment of order $3/2$ $\sigma_{3/2}$ (light blue), and mean absolute deviation σ_1 (purple) for one element of the Poiseuille flow model and for independent samples of increasing size M. The horizontal dotted line denotes the analytically computed value $\sigma_{3/2}^{(1)} \approx 0.820$. In the case $\alpha = 1$ we have $\sigma_1^{(1)} = 1/2$. Note that the figure was truncated with a maximum of 5 for the ordinate, while the standard deviation showed incursions up to 100.

Note again that, because we deal with times of flight (resulting from a single trajectory), the weighting is here naturally included in the statistics.

We propose to use the model (that allows for very large samples) in the simple case $n = 1$ to evaluate the reliability of this quantity: Figure 5 shows the evolution of the standard deviation $\sigma_2^{(1)}$ for increasing sample size M. For each sample we draw M times of flight, so that the samples are totally independent. As expected, the standard deviation does not converge but continues to increase with the sample size M, so that there is no limit value for this quantity, even if the divergence is very slow. What is more surprising is the fact that the signal is incredibly noisy: Indeed, while we show only data in the reduced vertical range $[0 : 5]$, values of up to 100 are present. Finally, although the fact that the different samples are independent may explain part of the randomness of the curve, we could expect at least the noise to decay when M increases. This is obviously not the case, which means that the standard deviation cannot even be used to compare two different laminar mixers using the same sample size. This point has to be stressed since, because of turbulent flows where distributions are close to Gaussian, nearly all RTD studies in fluid mechanics use this parameter (and sometimes higher moments) [36–40]. The difficulty lies indeed in the fact that a logarithmic divergence is extremely difficult to detect from a series of points. For an experiment also, the algebraic decay is impossible to monitor in practice, so that the tail—responsible for the logarithmic divergence—will not be fully taken into account, hiding the problem.

Since the moment of order 2, related to the standard deviation, is mathematically ill posed, we propose to use a centered

absolute moment of order α defined as

$$\sigma_\alpha^{(n)} = \left[\int_{t_{\min}^{(n)}}^{\infty} f_n(t) \left| \frac{t}{t_m^{(n)}} - 1 \right|^\alpha dt \right]^{1/\alpha}, \qquad (14)$$

where α is strictly less than 2 and can be fractional; fractional moments are indeed frequently used in physics for evaluation of heavy-tailed distributions [33]. In practice, it can also be calculated from a finite series of M values of time of flight, as done for the standard deviation. We obtain:

$$\sigma_\alpha^{(n)} = \left[\frac{1}{M} \sum_{j=1}^{M} \left| \frac{t_j}{t_m^{(n)}} - 1 \right|^\alpha \right]^{1/\alpha}. \qquad (15)$$

Here again, the weighting is already contained in the Lagrangian nature of the time of flight. Evaluating this quantity from points uniformly distributed at inlet is described later [see Eq. (22)].

B. Choice of α

In our case, taking $\alpha = 1.99$ would do fine in theory, since the integral would converge. However, as seen in Fig. 5, the signal is very noisy for $\alpha = 2$, and we expect the chosen quantity to converge reasonably rapidly with increasing M. We therefore propose to test two different values of α, namely $\alpha = 3/2$ and $\alpha = 1$. The moment of order 1 [41] is more specifically named "mean absolute deviation" in statistics. As for the usual standard deviation, we wish to evaluate the reliability of these quantities using one element of the model ($n = 1$). We denote $\sigma_\alpha \equiv \sigma_\alpha^{(1)}$: We will check that the series in Eq. (15) actually converge when increasing the size M of the sample, and compare how fast they converge toward the limit σ_α for the two values of α. We thus need an analytical expression of σ_α from the model flow, calculated from Eq. (14).

The case $\alpha = 1$ is straightforward and leads to $\sigma_1 = 1/2$ for the model flow. Matsui and Pawlas calculated existing fractional moments of Pareto functions using Laplace transforms [42]; the results are expressed in terms of the β function and the Gauss hypergeometric function. We give in Appendix C a classic analytical calculation: We obtain $\sigma_{3/2} \approx 0.820$ for the model flow, and we expect to find the same value numerically.

In Fig. 5 we show the evolution of these quantities as a function of the sample size M, using the same set of data already used for the standard deviation $\sigma_2^{(1)}$. While both moments converge toward the desired limits, the convergence is far more rapid in the case $\alpha = 1$. The signal is also much less noisy for the mean absolute deviation, obviously much less sensitive to the presence of very large residence times in the sample. Note finally that σ_1 is reasonably converged for a quite low sample size ($M \geqslant 10^3$–10^4).

C. Influence of molecular diffusion

Since the reason for the divergence of the standard deviation σ_2 is linked to the existence of arbitrary long residence times, we could wonder whether this phenomenon would be effectively observed when molecular diffusion is taken into account. Indeed, molecular diffusion would allow the fluid particle to change streamline, preventing very long residence times from being observed. In numerical simulations also,
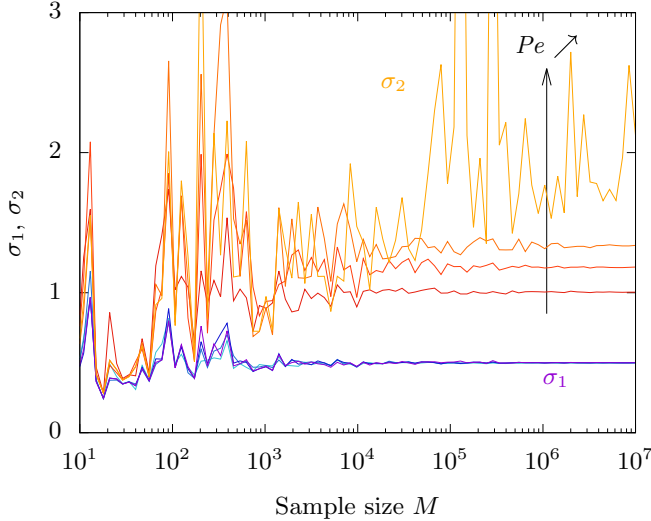
FIG. 6. Evolution of the standard deviation σ_2 (from red to yellow) and mean absolute deviation σ_1 (from blue to purple) for diffusing species in one element of the Poiseuille model flow, and independent samples of increasing size M. The Péclet numbers are Pe $= 10^6$, 10^7, 10^8, $+\infty$. The number of points is here much less than in Fig. 5, typically 15 samples in a decade compared to 150 in Fig. 5. Because molecular diffusion should not play a significant role in a single element of mixer, the different plateaus obtained for σ_2 are clearly artificial and show again that the standard deviation is ill posed here. In contrast, the mean absolute deviation σ_1 is nearly insensitive to molecular diffusion, proving that σ_1 is a robust measure of the width of RTD for a given mixer.

even without diffusion, the calculations would be stopped in the case of too-large residence times. This cutoff could enable the convergence of the standard deviation, and render this parameter acceptable for calculating the width of distributions. In order to evaluate how molecular diffusion would modify the preceding result, we proceed as follows: As for Fig. 5, we consider one element of the Poiseuille model flow, with length $L = D$, where D is the diameter of the entrance section. We define the Péclet number of the flow as Pe $= v_m D/D_s$, where D_s is the molecular diffusion of the species considered. The displacement of a given diffusing species obeys to

$$\frac{d\mathbf{x}}{dt} = \mathbf{v}(x, y, z, t) + \zeta(t), \tag{16}$$

where $\zeta(t)$ is a Gaussian decorrelated process such that $\langle \zeta_i(t)\zeta_j(t')\rangle = 2D_s\delta_{ij}\,\delta(t - t')$ [43]. For the model $\mathbf{v}$ is simply given by Eq. (1). As done in Fig. 5, for an abscissa M we generate M random initial locations with a parabolic probability. For those M initial points we solve Eq. (16) between $x = 0$ and $x = L$ for different realistic finite Péclet numbers (Pe $= 10^6$, 10^7, and 10^8), and also in the case without diffusion (Pe $= +\infty$); for each case we plot the standard deviation σ_2 and the mean absolute deviation σ_1 of the resulting RTD. As is visible in Fig. 6, σ_2 converges for finite Péclet number. However, the convergence is slow; even more important, the value of the plateau depends significantly on the Péclet number. Although we could expect a small dependence for a long mixer, those large differences for a single piece of mixer at high Péclet numbers are not physical, which shows that the
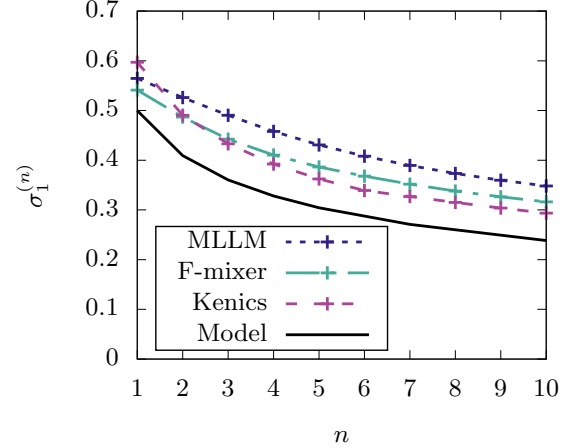

FIG. 7. Evolution of the mean absolute deviation $\sigma_1^{(n)}$ with the number of elements $n = 1, 2, 3, 4, 5, 7, 10$, for the three mixers and the model.

converged value obtained for σ_2 is artificial. In the case of σ_1, the curves merge for quite small samples, and, as expected in that situation, converge toward the theoretical value $\sigma_1 = 1/2$, whatever the Péclet number. This clearly shows that, unlike the standard deviation, the mean absolute deviation is a robust measure of the width of the distributions.

D. Application to the different mixers

Because the number of numerical data points used for the different mixers is in between 17 000 and 34 000, from the analysis above we have enough data to calculate reasonably accurately the mean absolute deviation,

$$\sigma_1^{(n)} = \frac{1}{M} \sum_{j=1}^{M} \left| \frac{t_j}{t_m^{(n)}} - 1 \right|. \tag{17}$$

Figure 7 shows $\sigma_1^{(n)}$ as a function of the number of elements for the three mixers and the model. In Appendix D, we show the same evolution for $\sigma_{3/2}^{(n)}$; we can check that the hierarchy between the different mixers is the same for the two different values of α, which definitely reinforces the choice $\alpha = 1$.

Without surprise, the totally uncorrelated model is the most efficient. As expected also, the reduced moment of the MLLM, which is the most correlated mixer, decreases less rapidly than the others; the Kenics is the best of the three mixers from the RTD point of view.

Although $\sigma_1^{(n)}$ is a decreasing function of n for all cases considered, there is no obvious analytical fit for the decay even in the case of the decorrelated model. The decrease is the most rapid at the beginning, for small values of n: The width of the distributions [measured with $\sigma_1^{(n)}$] has decreased by 25% (for the MLLM) to 40% (for the model) after $n = 5$ elements, but the decrease is only 40 to 52% for $n = 10$. Hence from the RTD point of view there is no interest in adding many elements in a row, provided that a good mixing is reached after a few number of elements.

V. INFLUENCE OF THE CROSS-SECTION GEOMETRY

In this section we would like to understand the reason for the differences in values of $\sigma_1^{(n)}$. Since large times of flight are linked to the presence of walls, one could wonder whether the shape of the mixer is of importance. As noted by Mortensen *et al.* [44], a shape can be characterized by a perimeter $\mathcal{P}$ and an area $\mathcal{A}$, that can be combined in a dimensionless compactness number $\mathcal{C}$, defined as

$$\mathcal{C} = \frac{\mathcal{P}^2}{\mathcal{A}}. \tag{18}$$

This quantity is not easy to measure for the mixers considered here. We thus propose to consider model flows as the one proposed in Sec. II C. We formerly took the case of a circular cross section, which allowed for analytical exact results easily comparable to numerical simulations. But it is relatively simple to investigate different compactness by varying the shape of the cross section (ellipse, square, or rectangle rather than a circle), as done in Mortensen *et al.* [44]. Because $\sigma_1^{(n)}$ decays roughly similarly with n for all mixers (Fig. 7), we focus on the value $n = 1$.

In the following we keep the area $\mathcal{A}$, length L and the flow rate $\mathcal{Q}$ constant, so that all different shapes correspond to the same mean time t_m.

A. Ellipse

There is no exact expression for the perimeter of an ellipse; however, it can be approximated using Ramanujan's second formula [45]:

$$\mathcal{P} \approx \pi(a+b)\left(1 + \frac{3\lambda^2}{10 + \sqrt{4 - 3\lambda^2}}\right) \text{ with } \lambda = \frac{a-b}{a+b}, \tag{19}$$

where a and b are the large and small semiaxes, respectively. This expression is very accurate, even for very elongated ellipses [46]. The parameter λ varies from 0 (circle) to 1 (very elongated ellipses). If $\mathcal{A} = \pi ab$ is kept constant, then $a + b = a + \mathcal{A}/(\pi a)$ is minimum for the circle; the bracketed expression in Eq. (19) is also a growing function of a, so that the perimeter is always increasing with a. The area $\mathcal{A}$ being kept constant, the compactness number $\mathcal{C}$ also increases with a.

However, as shown in Appendix E, the probability density of time duration for a pipe of length L is identical for a circular or elliptic cross section, whatever λ. This implies that all moments derived (including $\sigma_1^{(1)}$) are identical. In this case the compactness $\mathcal{C}$ plays no role on the distribution of duration times. Nevertheless, $\sigma_1^{(1)}$ may depend on the geometry, number of angles, etc.

B. Square and rectangles

Let us consider the Hagen-Poiseuille flow with rectangular cross section. The rectangle has a width a, a height b, and is characterized by its area $\mathcal{A} = a \times b$ and aspect ratio $\beta = b/a$. For this configuration, Spiga and Morino [47] proposed the
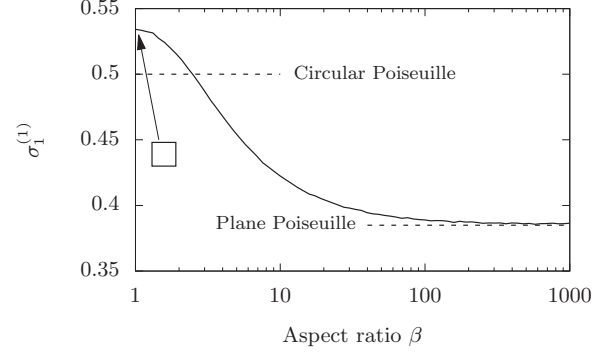

FIG. 8. Evolution of the mean absolute deviation for the Hagen-Poiseuille flow in rectangular ducts of varying aspect ratio β. Dashed lines indicate values of $\sigma_1^{(1)}$ for the circular and plane Poiseuille flow configurations, respectively, $\sigma_1^{(1)} = 1/2$ and $\sigma_1^{(1)} = 2/(3\sqrt{3}) \simeq 0.385$. As β increases, the configuration tends to that of the plane Poiseuille flow.

following expression for the velocity field:

$$v(y, z) = \frac{16a^2b^2G}{\mu\pi^4} \sum_{n \text{ odd}}^{\infty} \sum_{m \text{ odd}}^{\infty}$$
$$\frac{\sin[n\pi(y/a - 1/2)] \sin[m\pi(z/b - 1/2)]}{nm(b^2n^2 + a^2m^2)} \tag{20}$$

for $-a/2 \leqslant y \leqslant a/2$ and $-b/2 \leqslant z \leqslant b/2$, with G the imposed pressure gradient and μ the dynamic viscosity of the fluid. The mean velocity v_m is therefore:

$$v_m = \frac{64a^2b^2G}{\mu\pi^6} \sum_{n \text{ odd}}^{\infty} \sum_{m \text{ odd}}^{\infty} \frac{1}{n^2m^2(b^2n^2 + a^2m^2)}. \tag{21}$$

In practice, this series converges rather rapidly, and we checked that truncating the sums such that $0 \leqslant n, m \leqslant 1000$ was enough for our calculation. The aspect ratio is varied from $\beta = 1$ (square cross section) to $\beta = 1000$ (very elongated rectangle), the limit $\beta \to +\infty$ being the plane Poiseuille flow. Finally, all times are made nondimensional using the mean time $t_m = L/v_m$, where L is the length of the pipe section.

Due to the complexity of the expression of the velocity field, the inversion method is of no use in this situation. We can nonetheless compute the mean absolute deviation corresponding to this velocity field by taking points uniformly distributed in the rectangle and weighting the values using the velocity, which modifies expression (17) as follows:

$$\sigma_1^{(1)} = \frac{1}{M} \sum_{j=1}^{M} \frac{v_j}{v_m} \left| \frac{t_j}{t_m^{(1)}} - 1 \right|. \tag{22}$$

This approach was tested on the circular Poiseuille flow by taking points uniformly distributed on the disk and using the expression (22), and the same value of 0.5 was obtained for $\sigma_1^{(1)}$, confirming the validity of the method.

Figure 8 represents the evolution of $\sigma_1^{(1)}$ with the aspect ratio β. For each value of β, three samples of 100 000 points were computed, leading to slightly different values of $\sigma_1^{(1)}$ due to the randomness of the process. However, because of the rapid convergence of σ_1 with the sample size, the three

values are very close to each other, with a typical variation of order 0.5%; the quantity plotted in Fig. 8 is the mean for those three sets.

We observe that the mean absolute deviation decreases as the aspect ratio increases, converging to the value corresponding to the plane Poiseuille flow.

Note finally that in microfluidics, most microchannels have rectangular cross section; the case of the circular cross section, better than the square from the residence time point of view, is very close to the 3-1 rectangle, a geometry quite common in microfluidics.

VI. SUMMARY AND CONCLUSION

In this article we have studied the statistics of residence time distributions for n elements of an in-line mixer, using numerical data for three mixers and a model flow. We have shown that those types of mixers are not perfect from the RTD point of view and that the t^{-3} tail found for one element of mixer persists when increasing the number of elements. This algebraic decay, signature of a "heavy-tailed" distribution, has an important consequence in practice: The second-order moment of the distributions—and therefore higher moments—do not exist, so that the standard deviation cannot be used to characterize the width of the histogram.

Therefore we proposed to use the first-order absolute moment, also called mean absolute deviation, given by Eq. (17): This moment exists and converges with increasing sample size in numerical simulations and should also be used in experiments, where the tail is difficult to obtain in practice.

The mean absolute deviation is then used to compare the different mixers and how the typical width of the distribution decreases with n. It is also applied to discriminate between different shapes of cross section. We show that this parameter is higher for a square than for a circle but also that a rectangular cross section, very common in microfluidics, is a better mixer than a square from the RTD point of view.

One could wonder how the results for a mixer consisting of n elements would be affected by molecular diffusion. In fact, molecular diffusion has negligible effects as long as the Batchelor scale is not reached [48]. Since such in-line mixers reproduce the baker's map, the width of a given heterogeneity at the exit of the nth element is typically $\ell_n \sim w/2^n$, where w is the width of the cross section. Such an heterogeneity is mixed on a timescale $\tau_n \sim \ell_n^2/D_s$, where D is the molecular diffusion of the species to be mixed. Thus the scalar is mixed at the exit of the $(n + 1)$-th element if τ_n is of the order of the mean travel time in one element $t_m = L/v_m$. When equating $\tau_n \sim t_m$, we obtain

$$2n \ln 2 \sim \ln \left(\frac{v_m w}{D_s} \frac{w}{L} \right), \tag{23}$$

where we recognize the Péclet number $\text{Pe} = v_m w / D_s$. In an in-line mixer, the length L is a few times the width w (see Fig. 1), while the Péclet number is typically of the order of 10^6, so that $\ln(w/L)$ can be neglected in front of $\ln \text{Pe}$. We finally obtain

$$n \approx \frac{\ln \text{Pe}}{2 \ln 2}. \tag{24}$$

For $\text{Pe} = 10^6$, we obtain $n \approx 10$, so that in that case the effects of diffusion are negligible until the outlet of the mixer. In any case, even if the diffusion effects became important in the very last elements, this would not significantly change the statistics of the residence time on the whole mixer, so that our results should apply even if diffusion is taken into account.

APPENDIX A: GENERATION OF A RANDOM VARIABLE WITH PARABOLIC DENSITY

This basic technique is described in Ref. [26]. The goal is to derive a two-dimensional pdf that is proportional to the velocity field, here in the case of circular cross section:

$$f(M) \propto v(M) = v(r). \tag{A1}$$

By cylindrical symmetry, this is readily reduced to finding a one-dimensional pdf of the variable r, that has, however, to be proportional to the velocity field and the perimeter corresponding to the position considered:

$$f(r) \propto 2\pi r v(r) = 2\pi r \times 2v_m(1 - (r/R)^2). \tag{A2}$$

Since the integral of f over $[0, R]$ has to be 1, we easily obtain:

$$f(r) = \frac{4r}{R^2} \left(1 - \frac{r^2}{R^2} \right). \tag{A3}$$

We then compute the corresponding cumulative density function F, primitive of f:

$$F(r) = \frac{2r^2}{R^2} \left(1 - \frac{r^2}{2R^2} \right). \tag{A4}$$

Finally, the inverse function of F is expressed as:

$$F^{-1}(p) = R \sqrt{1 - \sqrt{1 - p}}, \quad \forall p \in [0, 1[. \tag{A5}$$

From here, the inversion method consists in generating a sample $(p_i)_{1 \leqslant i \leqslant M}$ of reals uniformly distributed between 0 and 1; in practice, we use a pseudorandom numbers generator (PRNG) to produce the uniform distribution, here the xoshiro256** PRNG of the gfortran compiler. We then apply F^{-1} to the sample produced. The result is a new sample of radii $(r_i)_{1 \leqslant i \leqslant M} = [F^{-1}(p_i)]_{1 \leqslant i \leqslant M}$ which follows the distribution law described by f.

APPENDIX B: TAIL OF RTD FOR n IDENTICAL ELEMENTS

Suppose that the RTD of 1 element of a mixer possesses a t^{-3} tail. Then, if the elements are decorrelated from the residence time point of view, then the tail of the distribution of n elements also has a t^{-3} tail.

Proof. We will proceed by recurrence. We denote by $f_m(t)$ the pdf associated to the crossing time for m sections. We

suppose that for all $m \leqslant (n-1)$, we have

$$f_m(t) = \frac{g_m(t)}{(t + t_\epsilon)^{-3}}, \tag{B1}$$

where t_ϵ is an arbitrary positive time and $g_m(t)$ a smooth function such as

$$g_m(t < m \times t_{\min}) = 0 \text{ and } \lim_{t \to \infty} g_m(t) = C_m \neq 0. \tag{B2}$$

The assertion (B2) is true for $n = 1$; we suppose that it is also true for $n - 1$ and prove that it is true for n. Providing that the events are sufficiently decorrelated, the pdf for n elements is the convolution product of f_1 with f_{n-1}:

$$
\begin{aligned}
f_n(t) &= \int_{-\infty}^{+\infty} f_1(t) \, f_{n-1}(t_n - t) \, dt \\
&= \int_{t_{\min}}^{t_n - (n-1)t_{\min}} \frac{g_1(t)}{(t + t_\epsilon)^3} \frac{g_{n-1}(t_n - t)}{(t_n + t_\epsilon - t)^3} \, dt.
\end{aligned} \tag{B3}
$$

We make the change of variable $x = t/t_n$, so that $dt = t_n \, dx$:

$$
\begin{aligned}
f_n(t) &= \int_{t_{\min}/t_n}^{1-(n-1)t_{\min}/t_n} \frac{g_1(t_n x)}{(t_n x + t_\epsilon)^3} \frac{g_{n-1}[t_n(1-x)]}{[t_\epsilon + t_n(1-x)]^3} t_n \, dx \\
&\underset{t_n \to \infty}{\sim} \int_0^1 t_n^{1-3-3} \frac{g_1(t_n x)}{(x + t_\epsilon/t_n)^3} \frac{g_{n-1}[t_n(1-x)]}{(t_\epsilon/t_n + 1 - x)^3} \, dx \\
&\underset{t_n \to \infty}{\sim} t_n^{-5} \int_0^1 \frac{g_1(t_n x)}{(x + t_\epsilon/t_n)^3} \frac{g_{n-1}[t_n(1-x)]}{(t_\epsilon/t_n + 1 - x)^3} \, dx
\end{aligned} \tag{B4}
$$

because of the presence of the constant t_ϵ, the function to integrate remains smooth on $[0; 1]$. Let us focus on Eq. (B4): When $t_n \to \infty$, we have $t_\epsilon/t_n \to 0$, and we have two important contributions, one at $x = 0$ and the other at $x = 1$. We thus neglect other contributions: In the vicinity of $x = 0$, the function to integrate is equivalent to $A_0 (x + t_\epsilon/t_n)^{-3}$, and in the vicinity of $x = 1$, is equivalent to $A_1(t_\epsilon/t_n + 1 - x)^{-3}$, where the fonctions that do not tend to infinity have been approximated by constants. We obtain:

$$f_n(t) \underset{t_n \to \infty}{\sim} t_n^{-5} \left[\frac{A_0}{2(t_\epsilon/t_n)^2} + \frac{A_1}{2(t_\epsilon/t_n)^2} \right], \tag{B5}$$

$$\underset{t_n \to \infty}{\sim} C_n \, t_n^{-3}. \tag{B6}$$

We have shown that $f_n(t)$ also has a t^{-3} tail and, by recurrence, the property is true for all n.

APPENDIX C: CALCULATION OF THE REDUCED MOMENT $\sigma_{3/2}^{(1)}$ FOR THE MODEL FOR ONE ELEMENT OF A CYLINDRICAL PIPE

The reduced moment $\sigma_{3/2}^{(1)}$ for one element of the model writes:

$$\sigma_{3/2}^{(1)} = \left(\frac{\sqrt{t_m}}{2} \int_{t_m/2}^{\infty} \frac{|t - t_m|^{3/2}}{t^3} \, dt \right)^{2/3}. \tag{C1}$$

Because of the absolute value, the integral is divided, one integral for $t \leqslant t_m$ (denoted by I_1) and the other for $t \geqslant t_m$

(denoted by I_2), such that

$$\sigma_{3/2}^{(1)} = (I_1 + I_2)^{2/3}. \tag{C2}$$

Calculation of $I_1(t \leqslant t_m)$

We set $u^2 = (1 - t/t_m)$. I_1 satisfies

$$I_1 = \int_0^{1/\sqrt{2}} \frac{u^4}{(1 - u^2)^3} \, du. \tag{C3}$$

We use formula 2.147(4) from Gradshteyn and Ryzhik [49]:

$$
\begin{aligned}
\int \frac{x^m \, dx}{(1 - x^2)^n} &= \frac{1}{2n - 2} \frac{x^{m-1}}{(1 - x^2)^{n-1}} \\
&\quad - \frac{m-1}{2n-2} \int \frac{x^{m-2} \, dx}{(1 - x^2)^{n-1}}
\end{aligned} \tag{C4}
$$

first with $m = 4$ and $n = 3$, next with $m = n = 2$ and obtain:

$$I_1 = -\frac{1}{4\sqrt{2}} + \frac{3}{8} \ln(\sqrt{2} + 1). \tag{C5}$$

Calculation of $I_2(t \geqslant t_m)$

We set $u^2 = (t/t_m - 1)$ and obtain:

$$I_2 = \int_0^{\infty} \frac{u^4}{(1 + u^2)^3} \, du. \tag{C6}$$

We next use formula 3.241(4) from Gradshteyn and Ryzhik [49]:

$$\int_0^{\infty} \frac{x^{\mu-1} \, dx}{(p + qx^\nu)^{n+1}} = \frac{1}{\nu p^{n+1}} \left(\frac{p}{q} \right)^{\mu/\nu} \frac{\Gamma(\mu/\nu) \, \Gamma(1 + n - \mu/\nu)}{\Gamma(1 + n)} \tag{C7}$$

with $\mu = 5$, $\nu = 2$, $p = q = 1$, and $n = 2$:

$$I_2 = \frac{1}{2} \frac{\Gamma(5/2) \, \Gamma(1/2)}{\Gamma(3)}, \tag{C8}$$

$$= \frac{3\pi}{16}. \tag{C9}$$

We finally obtain:

$$
\begin{aligned}
\sigma_{3/2}^{(1)} &= \left[-\frac{1}{4\sqrt{2}} + \frac{3}{8} \ln(\sqrt{2} + 1) + \frac{3\pi}{16} \right]^{2/3} \\
&\approx 0.820.
\end{aligned} \tag{C10}
$$

Ramsay [34] calculated fractional moments of this type of distribution using Laplace transforms, and gave the result in the form of an infinite series. We checked that the series indeed converged toward the same value.

APPENDIX D: EVOLUTION OF THE REDUCED MOMENT $\sigma_{3/2}^{(1)}$ WITH THE NUMBER OF ELEMENTS

The evolution of the reduced moment of order $3/2$ with the number n of elements is shown in Fig. 9. When compared to Fig. 7, the hierarchy between the different mixers is preserved; the decay with n is also similar.

APPENDIX E: FROM CIRCULAR TO ELLIPTIC CROSS SECTION: CALCULATION OF RTD FOR ONE ELEMENT OF MODEL MIXER

The velocity field for an ellipse of semiaxes a and b writes:

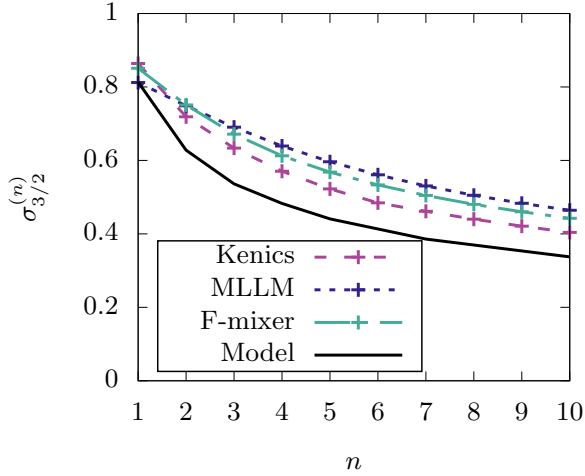$$v_x(y, z) = 2v_m \left(1 - \frac{y^2}{a^2} - \frac{z^2}{b^2} \right), \tag{E1}$$

FIG. 9. Evolution of $\sigma_{3/2}^{(n)}$ with the number of elements $n = 1, 2, 3, 4, 5, 7, 10$, for the three real mixers and the model.
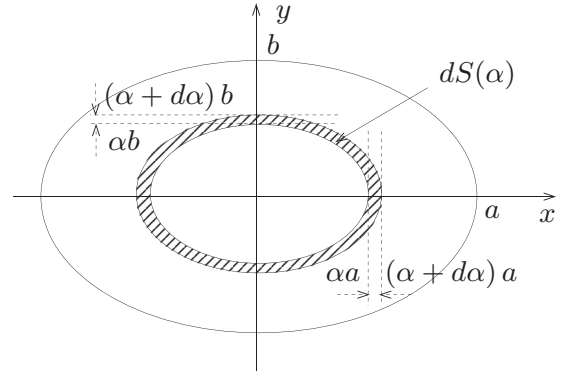

FIG. 10. Elliptic case: The hatched area represents the surface between the two ellipses corresponding to values α and $\alpha + d\alpha$ in Eq. (E4).

where v_m denotes the the mean velocity. We denote by $g(t)$ the density probability to have a time of flight of duration t for an element of size L, with

$$t = L/v_x(y, z) \, . \tag{E2}$$

Let us consider the points that verify

$$\frac{y^2}{a^2} + \frac{z^2}{b^2} = \alpha^2, \quad 0 \leqslant \alpha \leqslant 1 \, . \tag{E3}$$

They describe an ellipse of axes αa and αb. From Eqs. (E1), (E2), and (E3) we obtain

$$v_x(\alpha) = 2 v_m (1 - \alpha^2) = L/t \, , \tag{E4}$$

that differentiates into

$$4 \alpha \, d\alpha \, v_m = L \, dt/t^2 \, . \tag{E5}$$

Because the density probability is proportional to the velocity, we now write that the probability that t is in between t and $t + dt$ is the same as that for v_x to be in between $v_x(\alpha)$ and

$v_x(\alpha + d\alpha)$:

$$g(t) \, dt = \frac{v_x(\alpha)}{v_m} \frac{dS(\alpha)}{\pi \, ab} \, , \tag{E6}$$

with $dS(\alpha)$ the surface difference between ellipses corresponding to $\alpha + d\alpha$ and α, see Fig. 10. We thus have:

$$dS(\alpha) = \pi ab[(\alpha + d\alpha)^2 - \alpha^2]$$
$$\approx 2 \pi ab \, \alpha \, d\alpha \, . \tag{E7}$$

By combining equations (E4), (E5), (E6), and (E7), we obtain

$$g(t) = \frac{L}{v_m t} 2 \alpha \frac{d\alpha}{dt} \, , \tag{E8}$$

$$= \frac{L^2}{2 v_m^2 \, t^3} \, . \tag{E9}$$

The mean time t_m verifies

$$t_m = \frac{1}{\pi ab} \int_{\alpha=0}^{\alpha=1} \frac{v_x(\alpha)}{v_m} \times \frac{L}{v_x(\alpha)} \, dS(\alpha), \tag{E10}$$

$$= \frac{L}{v_m} \, . \tag{E11}$$

We finally obtain

$$g(t) = \frac{t_m^2}{2 \, t^3} \, , \tag{E12}$$

that is, the same expression as for the circle Eq. (11).

[1] J. M. Ottino, Mixing, chaotic advection, and turbulence, Annu. Rev. Fluid Mech. **22**, 207 (1990).

[2] H. Aref, J. R. Blake, M. Budišić, S. S. S. Cardoso, J. H. E. Cartwright, H. J. H. Clercx, K. El Omari, U. Feudel, R. Golestanian, E. Gouillart, G. F. van Heijst, T. S. Krasnopolskaya, Y. Le Guer, R. S. MacKay, V. V. Meleshko, G. Metcalfe, I. Mezić, A. P. S. de Moura, O. Piro, M. F. M. Speetjens, R. Sturman, J.-L. Thiffeault, and I. Tuval, Frontiers of chaotic advection, Rev. Mod. Phys. **89**, 025007 (2017).

[3] E. Gouillart, O. Dauchot, and J.-L. Thiffeault, Measures of mixing quality in open flows with chaotic advection, Phys. Fluids **23**, 013604 (2011).

[4] M. V. Budyansky, M. Yu. Uleysky, and S. V. Prants, Detection of barriers to cross-jet lagrangian transport and its destruction in a meandering flow, Phys. Rev. E **79**, 056215 (2009).

[5] S. Rossi, M. Petrelli, D. Morgavi, D. González-García, L. A. Fischer, F. Vetere, and D. Perugini, Exponential decay of concentration variance during magma mixing: Robustness of a volcanic chronometer and implications for the homogenization

of chemical heterogeneities in magmatic systems, Lithos **286**, 396 (2017).

[6] S. Wiggins and J. M. Ottino, Foundations of chaotic mixing, Phil. Trans. R. Soc. Lond. A **362**, 937 (2004).

[7] H. Bruus, *Theoretical Microfluidics*, Vol. 18 (Oxford University Press, Oxford, 2008).

[8] M. Creyssels, S. Prigent, Y. Zhou, X. Jianjin, C. Nicot, and P. Carrière, Laminar heat transfer in the "MLLM" static mixer, Int. J. Heat Mass Transf. **81**, 774 (2015).

[9] S. A. Bahrani, L. Humberset, R. Osipian, L. Royon, K. Azzouz, and A. Bontemps, How thermally efficient are chaotic advection mixers? An experimental assessment, Int. J. Therm. Sci. **145**, 106046 (2019).

[10] A. D. Stroock, S. K. W. Dertinger, A. Ajdari, I. Mezic, H. A. Stone, and G. M. Whitesides, Chaotic mixer for microchannels, Science **295**, 647 (2002).

[11] O. Gorodetskyi, M. F. M. Speetjens, P. D. Anderson, and M. Giona, Analysis of the advection–diffusion mixing by the mapping method formalism in 3D open-flow devices, AIChE J. **60**, 387 (2014).

[12] A. Borgogna, M. A. Murmura, M. C. Annesini, M. Giona, and S. Cerbelli, A hybrid numerical approach for predicting mixing length and mixing time in microfluidic junctions from moderate to arbitrarily large values of the Péclet number, Chem. Eng. Sci. **196**, 247 (2019).

[13] P. V. Danckwerts, Continuous flow systems: Distribution of residence times, Chem. Eng. Sci. **2**, 1 (1953).

[14] P. V. Danckwerts, Local residence-times in continuous-flow systems, Chem. Eng. Sci. **9**, 78 (1958).

[15] F. Raynal and P. Carrière, The distribution of "time of flight" in three dimensional stationary chaotic advection, Phys. Fluids **27**, 043601 (2015).

[16] F. Raynal, A. Beuf, and P. Carrière, Numerical modeling of DNA-chip hybridization with chaotic advection, Biomicrofluidics **7**, 034107 (2013).

[17] L. Oteski, Y. Duguet, and L. R. Pastur, Lagrangian chaos in confined two-dimensional oscillatory convection, J. Fluid Mech. **759**, 489 (2014).

[18] J.-P. Eckmann and D. Ruelle, Ergodic theory of chaos and strange attractors, in *The Theory of Chaotic Attractors* (Springer Science+Business Media, New York, 1985).

[19] R. Artuso, L. Cavallasca, and G. Cristadoro, Dynamical and transport properties in a family of intermittent area-preserving maps, Phys. Rev. E **77**, 046206 (2008).

[20] D. M. Hobbs, P. D. Swanson, and F. J. Muzzio, Numerical characterization of low Reynolds number flow in the Kenics static mixer, Chem. Eng. Sci. **53**, 1565 (1998).

[21] B. L. Gray, D. Jaeggi, N. J. Mourlas, B. P. van Drieënhuizen, K. R. Williams, N. I. Maluf, and G. T. A. Kovacs, Novel interconnection technologies for integrated microfluidic systems, Sens. Actuat. **77**, 57 (1999).

[22] P. Carrière, On a three-dimensional implementation of the baker's map, Phys. Fluids **19**, 118110 (2007).

[23] Z. Anxionnaz-Minvielle, P. Tochon, R. Couturier, C. Magallon, F. Théron, M. Cabassud, and C. Gourdon, Implementation of 'chaotic' advection for viscous fluids in heat exchanger/reactors, Chem. Eng. Process.: Process Intensif. **113**, 118 (2017).

[24] H. Chen and J.-S. Meiners, Topologic mixing on a microfluidic chip, Appl. Phys. Lett. **84**, 2193 (2004).

[25] Z. Chen, M. R. Bown, B. O'Sullivan, J. M. MacInnes, R. W. K. Allen, M. M. M. Blom, and R. van't Oever, Performance analysis of a folding flow micromixer, Microfluid. Nanofluid. **6**, 763 (2009).

[26] L. Devroye, *Non-Uniform Random Variate Generation* (Springer-Verlag, Berlin, 1986).

[27] W. Feller, *An Introduction to Probability Theory and Its Applications*, 2nd ed. (John Wiley & Sons, New York, 1971).

[28] C. Wilke, S. Altmeyer, and T. Martinetz, Large-scale evolution and extinction in a hierarchically structured environment, in *Proceedings of the 6th International Conference on Artificial Life* (MIT Press, Cambridge, MA, 1998), pp. 266–274.

[29] K. El Omari, E. Younes, T. Burghelea, C. Castelain, Y. Moguen, and Y. Le Guer, Active chaotic mixing in a channel with rotating arc-walls, Phys. Rev. Fluids **6**, 024502 (2021).

[30] L. B. Klebanov, *Heavy Tailed Distributions*, Vol. 488 (Matfyzpress, Prague, 2003).

[31] V. Pareto, *Cours d'Économie Politique*, Vol. 1 (Librairie Droz, Geneva, 1964).

[32] S. T. Rachev, *Handbook of Heavy Tailed Distributions in Finance: Handbooks in Finance, Book 1* (Elsevier, Amsterdam, 2003).

[33] T. Srokowski, Fractional Fokker-Planck equation for Lévy flights in nonhomogeneous environments, Phys. Rev. E **79**, 040104(R) (2009).

[34] C. M. Ramsay, The distribution of sums of certain I.I.D. pareto variates, Commun. Stat. Theory Methods **35**, 395 (2006).

[35] V. Larivière, V. Kiermer, C. J. MacCallum, M. McNutt, M. Patterson, B. Pulverer, S. Swaminathan, S. Taylor, and S. Curry, A simple proposal for the publication of journal citation distributions, bioRxiv 062109 (2016).

[36] J.-H. Ham and B. Platzer, Semi-empirical equations for the residence time distributions in disperse systems—Part 1:Continuous phase, in *Chemical Engineering & Technology: Industrial Chemistry, Plant Equipment, Process Engineering, and Biotechnology*, Vol. 27 (WILEY-VCH Verlag GmbH & Co. KGaA, Weinheim, 2004), 1172.

[37] F. Trachsel, A. Günther, S. Khan, and K. F. Jensen, Measurement of residence time distribution in microfluidic systems, Chem. Eng. Sci. **60**, 5729 (2005).

[38] J. T. Adeosun and A. Lawal, Numerical and experimental studies of mixing characteristics in a T-junction microchannel using residence-time distribution, Chem. Eng. Sci. **64**, 2422 (2009).

[39] D. Bošković, S. Loebbecke, G. A. Gross, and J. M. Koehler, Residence time distribution studies in microfluidic mixing structures, Chem. Eng. Technol. **34**, 361 (2011).

[40] A. E. Rodrigues, Residence time distribution (RTD) revisited, Chem. Eng. Sci. **230**, 116188 (2021).

[41] U. Khair, H. Fahmi, S. Al Hakim, and R. Rahim, Forecasting error calculation with mean absolute deviation and mean absolute percentage error, J. Phys.: Conf. Ser. **930**, 012002 (2017).

[42] M. Matsui and Z. Pawlas, Fractional absolute moments of heavy tailed distributions, Braz. J. Probab. Stat. **30**, 272 (2016).

[43] H. Aref and S. W. Jones, Enhanced separation of diffusing particles by chaotic advection, Phys. Fluids **1**, 470 (1989).

[44] N. A. Mortensen, F. Okkels, and H. Bruus, Reexamination of hagen-poiseuille flow: Shape dependence of the hydraulic resistance in microchannels, Phys. Rev. E **71**, 057301 (2005).

[45] S. Ramanujan, *Ramanujan's Collected Works* (Chelsea, New York, 1962).

[46] M. B. Villarino, Ramanujan's perimeter of an ellipse [https://arxiv.org/abs/math/0506384].

[47] M. Spiga and G. L. Morino, A symmetric solution for velocity profile in laminar flow through rectangular ducts, Int. Commun. Heat Mass Transf. **21**, 469 (2006).

[48] F. Raynal and J.-N. Gence, Energy saving in chaotic laminar mixing, Int. J. Heat Mass Transf. **40**, 3267 (1997).

[49] I. S. Gradshteyn and I. M. Ryzhik, *Table of Integrals, Series, and Products*, 7th ed. (Elsevier/Academic Press, Amsterdam, 2007).